Brain Research Bulletin 176 (2021) 54–66

Contents lists available at ScienceDirect

Brain Research Bulletin

journal homepage: www.elsevier.com/locate/brainresbull

Acute administration of sulfur-doped g-C3N4 induces cognitive deficits and exacerbates the levels of glial activation in mouse hippocampus

Farangis Ramezani [a], Maryam Ghasemi-Kasman [b,c,*], Nasrin Nosratiyan [a], Shahram Ghasemi [d], Farideh Feizi [b]

[a] Student Research Committee, Babol University of Medical Sciences, Babol, Iran
[b] Cellular and Molecular Biology Research Center, Health Research Institute, Babol University of Medical Sciences, Babol, Iran
[c] Neuroscience Research Center, Health Research Institute, Babol University of Medical Sciences, Babol, Iran
[d] Faculty of Chemistry, University of Mazandaran, Babolsar, Iran

ARTICLE INFO

Keywords:
Sulfur-doped g-C3N4
Neurotoxicity
Spatial memory
Hippocampus
Neuronal loss

ABSTRACT

During the last decades, graphitic carbon nitride (g-C3N4) has attracted increasing attention in several biomedical fields. In this study, the effects of sulfur-doped g-C3N4 (TCN) on cognitive function and histopathology of hippocampus were investigated in mice. The characteristics of synthetized sample were evaluated by X-ray diffraction (XRD), Fourier transform infrared spectroscopy (FT-IR), Raman spectroscopy, transmission electron microscopy (TEM), field emission scanning electron microscopy (FESEM), and energy dispersive X-ray (EDX). Twenty-four male NMRI mice received vehicle, TCN at doses of 50, 150, or 500 mg/kg *via* gavage for one week. Morris water maze test was done to assess the cognitive function at day 14 post TCN administration. Nissl staining was used to determine the number of dark cells in the hippocampus. Immunostaining against NeuN, GFAP, and Iba1 was done to evaluate the neuronal density and levels of glial activation, respectively. Behavioral tests indicated that TCN reduces the spatial learning and memory in a dose-dependent manner. Histological evaluations showed an increased level of neuronal loss and glial activation in the hippocampus of TCN treated mice at doses of 150 and 500 mg/kg. Overall, our data indicate that TCN induces the cognitive impairment that is partly mediated *via* its exacerbating impacts on neuronal loss and glial activation.

1. Introduction

Nanotechnology has emerged as a promising approach in several biomedical fields (Bhardwaj and Kaushik, 2017). Among the wide range of nanostructures, carbon-based nanomaterials, due to their unique chemical and physical properties, have been extensively explored for their potential applications and shown revolutionary success in various fields (Karmakar et al., 2014; Loh et al., 2018; Xiong et al., 2017). Graphene and its derivatives, carbon nanotube and carbon nitride have recently become frontline carbon nanomaterial in diagnostic and therapeutic purposes, including drug and gene delivery, cancer treatment, tissue engineering, and bio sensing (Chan et al., 2019; Teradal and Jelinek, 2017; Wang and Yang, 2019; Xiong et al., 2017). Their small size enables them to be internalized by cells in either a therapeutic or toxic manner (Baldrighi et al., 2016; Teleanu et al., 2019). Their conjugation capacity with drugs and nucleic acids, and the modifiable surface properties, introduce them as cell-specific and disease-specific drug vehicles (Maiti et al., 2019; Mohajeri et al., 2019).

Considering the variety in applications of carbon-based nanomaterials, safety assessments are prerequisite for their clinical applications in therapy. Several toxicological assays on carbon nanotube have shown that it can induce cytotoxicity in the lung, liver, spleen, kidney, and CNS after crossing the biological barriers, cellular uptake, and intracellular localization (Amrollahi-Sharifabadi et al., 2018; Baldrighi

Abbreviations: CNS, central nervous system; BBB, blood brain barrier; g-C3N4, graphitic carbon nitride; AD, Alzheimer's disease; TCN, sulfur-doped g-C3N4; XRD, X-ray diffraction; FT-IR, Fourier-transform infrared spectroscopy; FESEM, field emission scanning electron microscope; TEM, transmission electron microscopy; EDX, energy dispersive X-ray; GO, graphene oxide; MWM, Morris water maze; H&E, hematoxylin and eosin; PBS, phosphate buffered saline; PFA, paraformaldehyde; Gfap, glial fibrillary acidic protein; Iba1, ionized calcium binding adaptor molecule 1; NGS, normal goat serum; DAPI, 4′, 6-diamidino-2 phenylindole; ANOVA, analysis of variance; CNT, carbon nanotube.

* Corresponding author at: Babol University of Medical Sciences, P.O. Box 4136747176, Babol, Iran.
E-mail address: m.ghasemi@mubabol.ac.ir (M. Ghasemi-Kasman).

https://doi.org/10.1016/j.brainresbull.2021.08.006
Received 14 June 2021; Received in revised form 29 July 2021; Accepted 15 August 2021
Available online 19 August 2021

et al., 2016; Fisher et al., 2012). Different biocompatibility studies reported neuronal damage, and behavioral consequences following carbon nanostructures exposure (Liu et al., 2014; Sayapina et al., 2017, 2016; Shi et al., 2017; Weber et al., 2014). Hence the feasibility of their clinical application remains a matter of debate.

A recently introduced carbon nanomaterial, graphitic carbon nitride (g-C3N4), has become a hotspot in current researches. Its high photoluminescence activity and considerable chemical and thermal stability have been widely explored for assessing the presumptive clinical applications (Shi et al., 2017; Tian et al., 2013; Weber et al., 2014). Although the photocatalytic activity of pure g-C3N4 is very low because of fast recombination rate of photogenerated electron-hole pairs and limited utilization of solar energy (Cao et al., 2015; Tian et al., 2014). Various strategies have been developed to improve the photocatalytic performance of g-C3N4. Doping has been introduced as an efficient and facile method for increasing the photocatalytic efficiency (Wang et al., 2018). Interestingly, it has been shown that doping with nonmetal element S effectively enhances the photocatalytic activity of g-C3N4 (Ge et al., 2013; Liu et al., 2010).

The graphitic carbon nitride has shown desirable function in various biomedical fields, particularly in brain targeting strategies (Xiong et al., 2017; Zhang et al., 2020). Conferring with pathologic biomolecules in Alzheimer's disease (AD) as a nanochelator, its excellent photodynamic activity against cancer cells and remarkable bio sensing and drug-carrying potential are generally considered the most superior features for biomedical applications (Wang et al., 2016; Wang and Yang, 2019; Zhang et al., 2013, 2010).

Despite its favorable characteristics, g-C3N4's toxicological evaluations are at their preliminary stages. I*n vitro* assessments are mostly agreed on dose-dependent toxic effects (Chu et al., 2017; Chung et al., 2016; Dong et al., 2018). It is worth mentioning that some studies reported no alteration in the viability of g-C3N4 incubated cells even with high concentrations of this nanostructure, which suggests its good biocompatibility (Li et al., 2016; Rong et al., 2016; Zhang et al., 2013).

To the best of our knowledge, almost all biocompatibility assessments of g-C3N4 were carried out *in vitro*. Hence its probable toxic behavior is largely unknown. Some *in vitro* assessments have shown that g-C3N4 may be able to functionally and histologically alter various organs of living organisms after exposure (Dong et al., 2018). This is a critical issue in the CNS considering brain targeting applications of g-C3N4 in addition to unintentional exposure of brain following g-C3N4 administration for any other purposes.

According to previous toxicological evaluations, cellular inflammatory responses may play a key role in cellular changes after being exposed to carbon nanostructures (Amrollahi-Sharifabadi et al., 2018; Baldrighi et al., 2016). Focusing on the brain, glial activation is one of the key elements in generating inflammatory conditions (Bardi et al., 2013). Previous experiments have shown that activation of astrocytes and microglial cells followed by secretion of inflammatory mediators is majorly associated with carbon nanostructures related neuroinflammatory responses. Hence, it is vital to trace glial cells activity to gain a better insight into neural impacts of g-C3N4 (Bardi et al., 2013; Belyanskaya et al., 2009; Bussy et al., 2015).

Here, we focused on the short-term effect of sulfur-doped g-C3N4 (TCN) as the initial step of figuring TCN toxicological behavior *in vivo*. To this end, the impact of one-week administration of TCN on spatial learning and memory was examined in mice. Furthermore, the levels of hippocampal neuronal loss and glial activation were evaluated using histological staining.

2. Materials and methods

2.1. Synthesis of S-doped g-C3N4

The sulfur-doped g-C3N4 was prepared by a facile and efficient heating method based on a previous report (Cao et al., 2015). In brief, 2 g of thiourea was placed in an alumina crucible with a cover, and then heated at 550 °C for 2 h. After that, it was slowly cooled down to the room temperature and the resultant yellow sample was collected and grounded into powders.

2.2. Characterization of S-doped g-C3N4

The phase composition of synthetized S-doped g-C3N4 was analyzed by X-ray diffraction (XRD PW1730, PAN analytical, Netherlands) in the angular region of $2\theta = 10°–70°$. Fourier-transform infrared spectroscopy (FT-IR) spectra and Raman spectra were recorded by FT-IR AVATAR (Thermo Company, USA) and Teksan system (TakRam N1-541, Iran), respectively. The morphology and topography of obtained g-C3N4 were examined by field emission scanning electron microscope (FESEM MIRA III, TESCAN, Czech Republic) and transmission electron microscopy (TEM, CM120, Netherlands) at 100 Kv. Energy dispersive X-ray (EDX) analysis was performed (FESEM MIRA II, TESCAN, Czech Republic) using a SAMX detector (France).

2.3. Animals

Twenty-four male NMRI mice (age: 6–8 weeks; weight: 25−35 g) from animal house of Babol University of Medical Sciences (Babol, Iran) were used in the present study. The mice were kept in a standard animal room with free access to food and water. All experimental procedures were approved by the local ethics committee of Babol University of Medical Sciences (Approval No: IR.MUBABOL.REC.1399.252).

2.4. Experimental groups

Animals were randomly divided into four groups as follows (n = 6/group):

Group 1 as vehicle group: In this group, mice orally received 5 mL/kg of ethanol (5 % solution) as solvent of TCN for one week (Gad et al., 2006).

Groups 2−4: Mice were orally treated by TCN at doses 50, 150 or 500 mg/kg for one week (Amrollahi-Sharifabadi et al., 2018).

Two weeks after receiving the relevant interventions, the spatial learning and memory of mice were assessed using Morris water maze (MWM). Then, the levels of neuronal loss and astrocytes activation were examined by Nissl staining and immunostaining.

The experimental protocol was based on a toxicity study on graphene oxide (GO), which is structurally analogous to g-C3N4. The mentioned study was designed to investigate the acute administration of GO in the mice. The total doses of exposure were selected by chemical evaluation on GO nanostructure (Amrollahi-Sharifabadi et al., 2018).

2.5. Morris water maze test

In order to evaluate the spatial learning and memory of mice, the MWM test was used, as we have mentioned in our previous report (Hashemian et al., 2017). In brief, all mice were given four 60 s trials per day and this procedure was continued until day 4. On day 5, the hidden platform was removed from the water pool and mice were allowed to swim freely for 60 s. All results were recorded by a computer targeting system (HVS image 2020). The time to find the hidden platform (escape latency), distance moved, and times spent in the target quadrant were analyzed for each mouse.

2.6. Histological staining

The effect of TCN administration on hippocampal dark cells and histopathology of hippocampus were examined using Nissl staining and Hematoxylin and eosin (H&E) staining. In brief, mice were anesthetized using ketamine (70 mg/kg) and xylazine (10 mg/kg), and then, perfused with phosphate buffered saline (PBS) and 4 % paraformaldehyde (PFA).

After paraffin embedding, coronal sections (6 μm) were cut using a microtome (Leica RM2135, Germany). Based on our previous reports, cresyl violet (Merck, Germany) (Gol et al., 2017) and H&E (Naeimi et al., 2018) staining were done on prepared sections. The slides were evaluated under an Olympus IX71 microscope (Japan) and images from CA1 and CA3 regions of the hippocampus were captured by a DP-27 camera (Olympus, Japan).

2.7. Immunostaining

Immunostaining against glial fibrillary acidic protein (GFAP) as an astrocyte marker, ionized calcium binding adaptor molecule 1 (Iba1) as a microglia/macrophage-specific calcium-binding protein, and NeuN as a neuronal marker were used to assess the levels of hippocampal glial activation and neuronal loss, respectively (Hashemian et al., 2017).

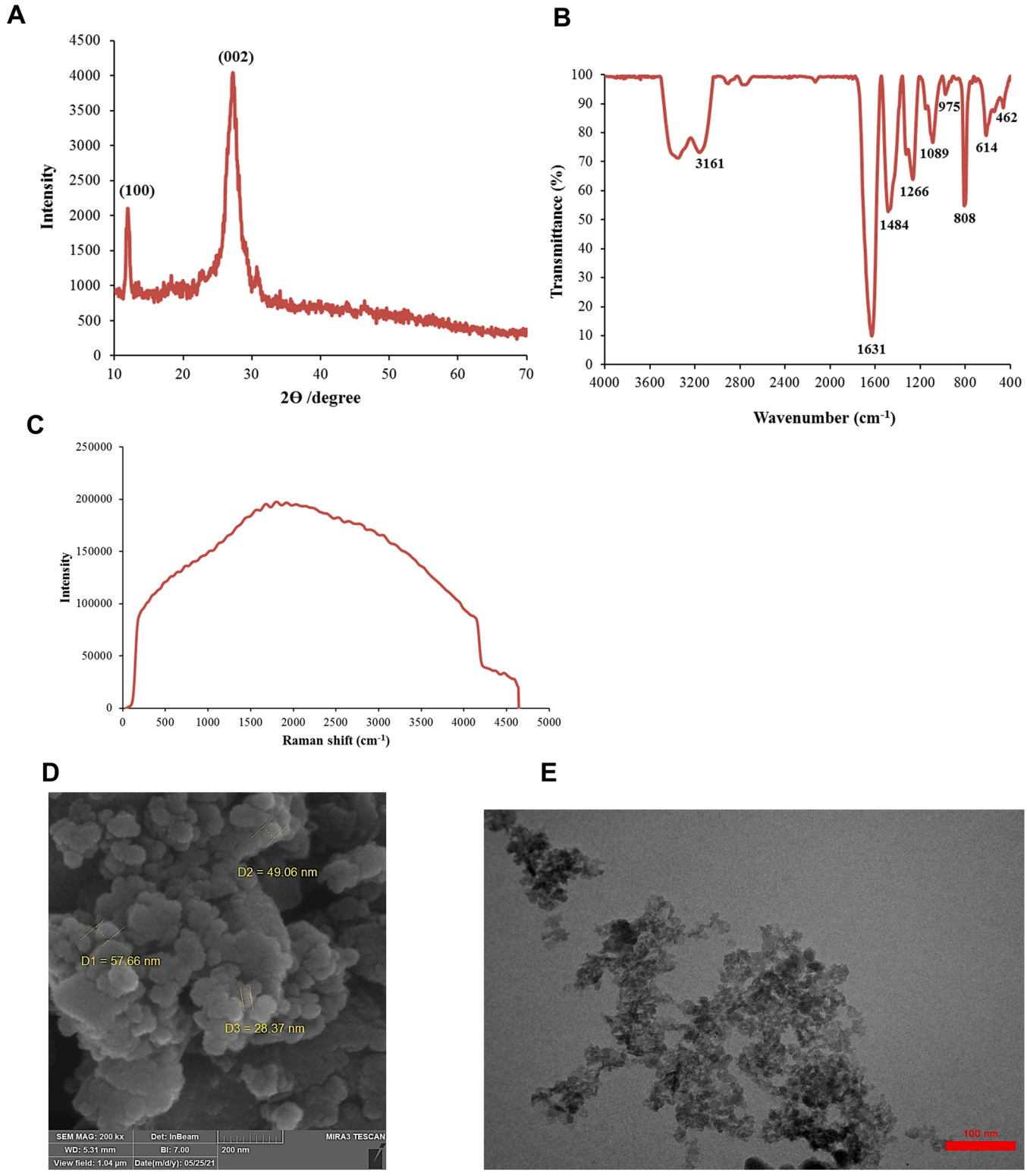

Fig. 1. A) XRD pattern for sulfur-doped g-C3N4. B) FT-IR spectra of the sulfur-doped g-C3N4. C) Raman spectra for sulfur-doped g-C3N4. FESEM (D) and TEM (E) images of sulfur-doped g-C3N4.

In brief, frozen coronal sections (6 μm) were rinsed with PBS for three times. In order to block non-specific bindings, hippocampal sections were incubated with normal goat serum (NGS) 10 % in 0.3 % Triton-X100 for 1 h. Then, the primary antibodies including rabbit anti-GFAP (1:400, Dako, Denmark), rabbit anti-Iba1 (1:500, Wako, USA) or rabbit anti-NeuN (1:500, Abcam, UK) were added and slides were put at 4 °C overnight. After rinsing with PBS for three times, the secondary antibodies as anti-rabbit IgG conjugated with Alexa 594 (1:1000, Abcam, UK) and anti-rabbit IgG conjugated with Alexa 488 (1:1000, Abcam, UK) were added and tissue sections were incubated for 1 h at room temperature. After that, the washing step was performed using PBS for 3 times and 4′,6-diamidino-2-phenylindole (DAPI) was used for nuclear staining. The prepared slides were evaluated under Smart Flow microscope (Canada) and images were taken from CA1 and CA3 regions

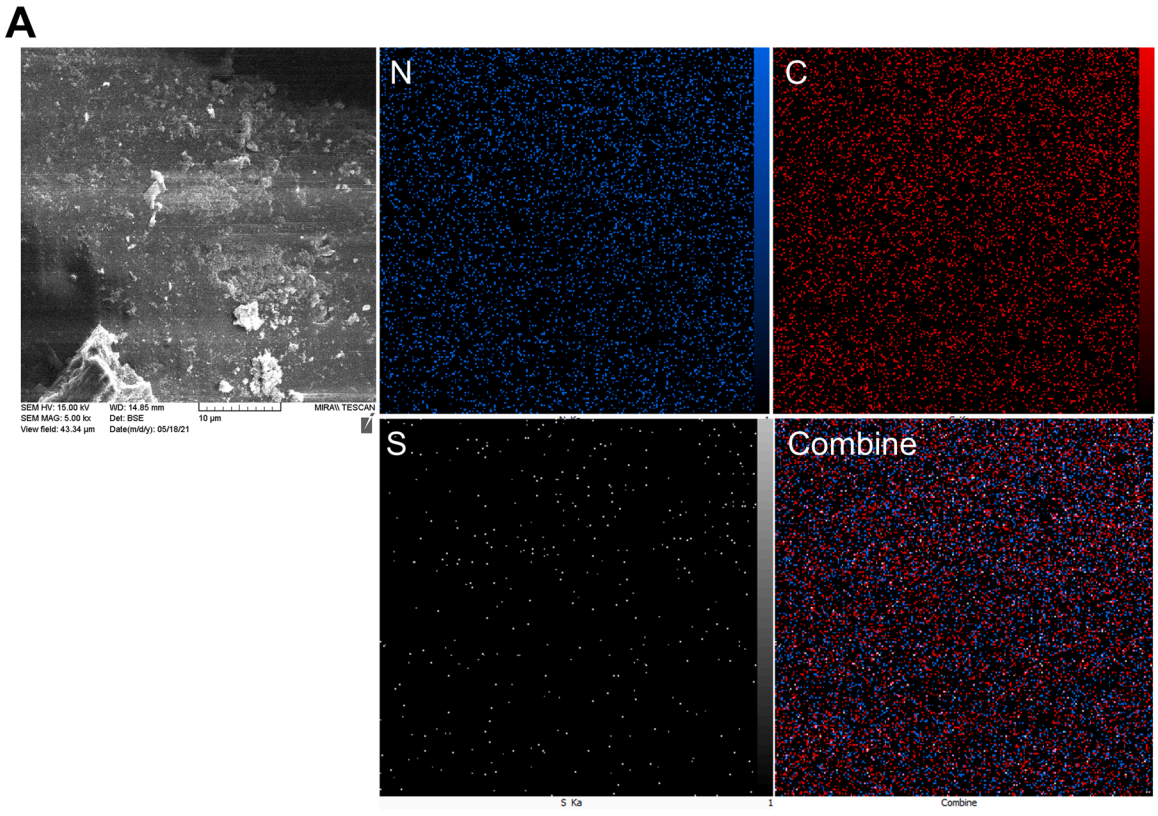

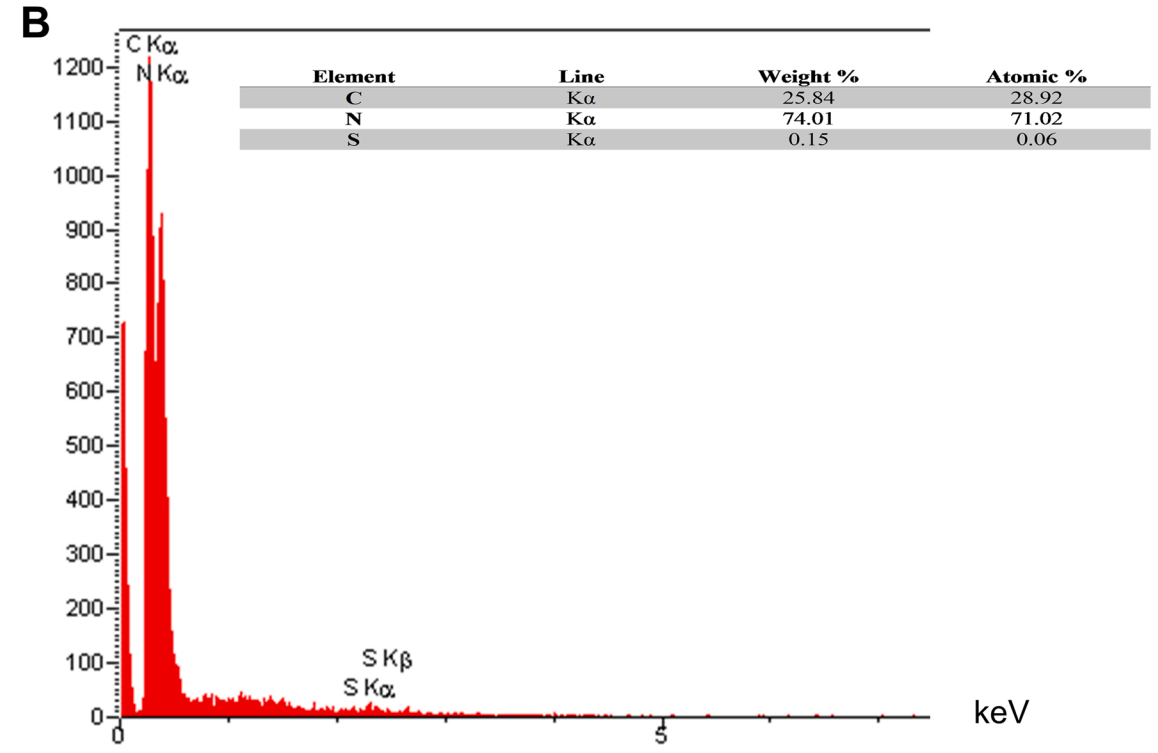

Element	Line	Weight %	Atomic %
C	Kα	25.84	28.92
N	Kα	74.01	71.02
S	Kα	0.15	0.06

Fig. 2. EDX analysis of sulfur-doped g-C3N4. Map (A) and quantification of EDX analysis.

of the hippocampus by CCD camera. Cell counting was done using Image J software 1.42 V (National Institutes of Health, USA). The number of GFAP^{+}, Iba1^{+}, and NeuN $^{+}$ cells was counted using Image J software 1.42 V (National Institutes of Health, USA) and averaged from three sections in each slide and three slides from each animal (Hashemian et al., 2019).

2.8. Statistical analyses

GraphPad Prism (version 6) was used for data analysis. The escape latency and distance moved parameters were analyzed by repeated measures two-way analysis of variance (ANOVA) and Bonferroni post-hoc. The analysis of probe test and histological data were done using

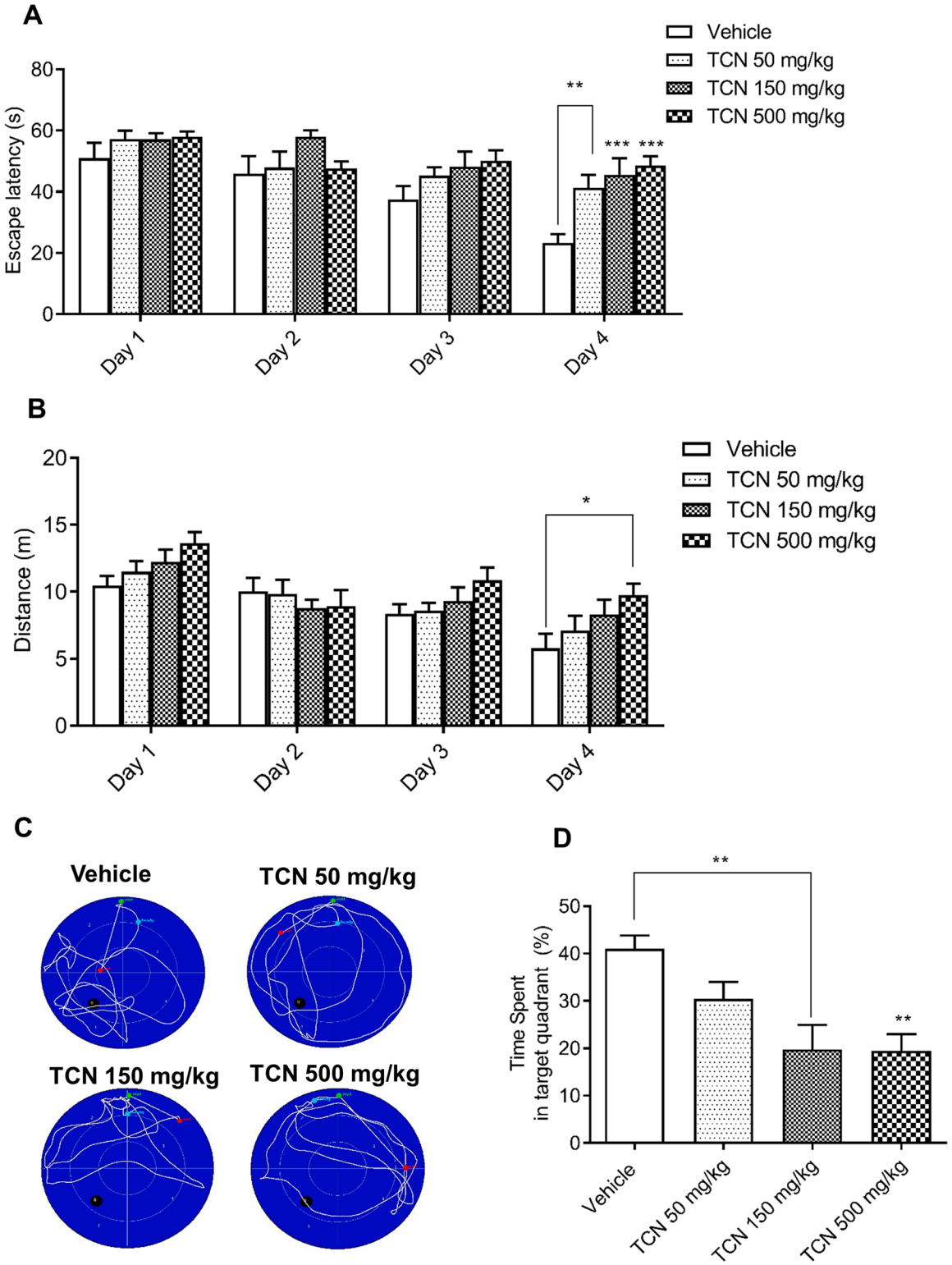

Fig. 3. Effect of TCN on learning ability and spatial memory of mice. The impacts of TCN on A) Escape latency and B) Traveled distance were assessed by Morris water maze test. C) Representative tracks for all experimental groups in the probe test. D) The results of probe test indicated that TCN dose dependently reduced the percentage of time spent in target quadrant. *P < 0.05, **P < 0.01, and ***P < 0.001 compare with vehicle, n = 6.

One-way ANOVA, followed by Bonferroni post-hoc. The results were expressed as mean ± SEM and $p < 0.05$ was considered statistically significant.

3. Results

3.1. Characterization

Fig. 1A shows the XRD pattern of prepared S-doped g-C3N4. In accordance with previous studies (Cao et al., 2015; Zhang et al., 2012), there are also two distinct diffraction peaks located at around 13.01 and 27.41, which can be indexed as (100) and (002) planes, respectively. The first peak is related to the in-plane ordering of tri-s-triazine units and the second peak corresponding to an interlayer-stacking distance of 0.326 nm (Cao et al., 2015).

FT-IR spectroscopy was used to examine the surface functionalities and chemical bonding in the prepared samples. The FT-IR spectrum of S-doped g-C3N4 reveals that the main peak appearing in 800 cm^{-1} is corresponded to triazine. In the range of 1200 to 1625 cm^{-1}, peaks related to C—N heterocyclic bonds are found. In addition, peaks related to the N—H bond can be observed in the range of 3000 to 3500 cm^{-1} (Vinoth et al., 2020) (Fig. 1B).

Raman spectrum of S-doped g-C3N4 showed a wide peak in the range of 0 to 4500 cm^{-1} and maximum intensity was about 1800 cm^{-1} (Fig. 1C).

The morphological and microstructural characterization of the prepared sample is presented in Fig. 1D, E. The FESEM image in Fig. 1D exhibits aggregated microstructures containing a large number of irregular particles with diameters ranging from 30 to 50 nm. TEM image showed that the S-doped g-C3N4 was grainy in structure (Fig. 1E).

The EDX-MAP analysis of obtained sample is presented in Fig. 2A, B. The results of EDS spectrum indicated that the synthetized product contains C, N, and S around 28.92 %, 71.02 % and 0.06 %, respectively. Interestingly, identification of X-ray characteristic lines related to sulfur (S Kα and S Kβ) confirms the presence of sulfur in g-C3N4 structure.

3.2. Acute administration of TCN reduces the spatial learning and memory of mice

In order to determine the effect of TCN on spatial learning and memory, MWM test was employed 2 weeks after administration of TCN. Based on learning ability of animals, the time for finding the hidden platform was reduced in vehicle group during training phase. A significant difference in escape latency was observed between TCN treated mice at dose of 50 mg/kg compared to the vehicle group at day 4 ($P = 0.007$). Additionally, the time for reaching the hidden platform was significantly increased in TCN received mice at doses 150 ($P = 0.0006$) and 500 mg/kg (<0.0001) compared to the vehicle group on day 4 (Fig. 3A).

Analysis of MWM results also showed that the traveled distance significantly increased in TCN treated mice at dose of 500 mg/kg compared to the vehicle on day 4 ($P = 0.02$) (Fig. 3B). No significant difference in traveled distance was observed between other experimental groups.

In order to evaluate the effect of TCN on spatial memory, probe test was carried out on day 5. Fig. 3C shows the representative tracks for all experimental groups. Analysis of probe data showed that the percentage of time spent in target quadrant significantly reduced in TCN received mice at dose of 150 mg/kg compared to the vehicle ($P = 0.005$). In addition, a significant decrease in crossing former platform site was observed in TCN treated mice at dose of 500 mg/kg compared to the vehicle ($P = 0.005$) (Fig. 3D).

3.3. Acute administration of TCN increases the hippocampal dark cells

Analysis of Nissl staining data showed the number of pyknotic cells significantly increased in CA1 area of TCN treated mice at doses of 150 ($P = 0.004$) and 500 mg/kg ($P < 0.0001$) compared to the vehicle. A significant increase in level of pyknotic cells was also observed in TCN groups at doses of 150 ($P = 0.01$) and 500 mg/kg ($P < 0.0001$) compared to the TCN at dose of 50 mg/kg. Our data indicated that the number of dark neurons markedly increase in CA1 region of TCN treated mice at dose of 500 mg/kg compared to dose of 150 mg/kg ($P = 0.004$) (Fig. 4A, C).

Analysis of Nissl staining data in CA3 region also demonstrated that acute administration of TCN at doses of 150 ($P = 0.0005$) and 500 mg/kg ($P < 0.0001$) markedly increase the number of dark neurons compared to the vehicle. In comparison to TCN at dose of 50 mg/kg, the number of pyknotic cells was significantly increased in CA3 area of TCN treated mice at doses of 150 ($P = 0.002$) and 500 mg/kg ($P = 0.0002$) (Fig. 4B, D).

3.4. Acute administration of TCN increases the hippocampal neuronal loss

To evaluate the possible impact of TCN on hippocampal neuronal loss, immunostaining against NeuN as mature neuronal marker was conducted in CA1 and CA3 regions of hippocampus. Quantification of immunostaining results showed that the number of NeuN positive cells was not significantly changed in CA1 region of TCN treated mice at dose of 50 mg/kg compared to the vehicle group. The intensity of NeuN was markedly decreased in TCN treated mice at doses of 150 ($P = 0.001$) and 500 mg/kg ($P = 0.0005$) compared with vehicle. A significant difference in number of NeuN expressing cells was also observed between TCN 50 and 500 mg ($P = 0.02$) (Fig. 5A, B).

Analysis of immunostaining data in CA3 region also indicated that level of neuronal loss significantly increased in TCN treated mice at doses of 50 ($P = 0.02$), 150 ($P < 0.0001$), and 500 mg/kg ($P < 0.0001$) compare with vehicle. A significant difference in number of NeuN positive cells was also found in TCN treated mice at dose of 50 compare to doses of 150 ($P = 0.001$), and 500 mg/kg ($P = 0.001$) (Fig. 5C, D).

3.5. The effect of TCN administration on histopathology of hippocampus

In order to determine the impact of TCN administration on histopathology of hippocampus, the hippocampal sections were evaluated by H&E staining. As Fig. 6 shows the hippocampal pyramidal cells in the CA1 and CA3 regions of vehicle group are mostly regular and have pale nuclei. In contrast, in the TCN-receiving groups, irregularities in cell placement and necrotic changes, including nucleus aggregation, were observed in a dose-dependent manner. Hyperemia, cytoplasm vacuolation, and accumulation of degenerated cells were also found in the TCN-receiving mice.

3.6. Acute administration of TCN exacerbates the hippocampal glial activation

To examine the possible effect of TCN on astrocytes activation, the level of astrocytes activation was evaluated using GFAP immunostaining in the CA1 and CA3 regions of hippocampus. Although the number of GFAP expressing cells was significantly increased in TCN treated mice at dose of 50 mg/kg compare with vehicle, but this difference was not significant. Our data showed the level of astrocytes activation was markedly increased in TCN received mice at dose of 150 mg/kg compare with vehicle ($P = 0.002$). Furthermore, a remarkable morphological changes that are characterized with thick processes of astrocytes, was found in CA1 region of TCN treated mice at dose of 500 mg/kg. The number of GFAP positive cells was markedly increased in CA1 region of TCN treated mice at dose of 500 mg/kg compare with vehicle ($P = 0.001$) and TCN at dose of 50 mg/kg ($P = 0.01$) (Fig. 7A, B).

Our data also showed that the number of GFAP expressing cells significantly increased in CA3 region of TCN received mice at doses of

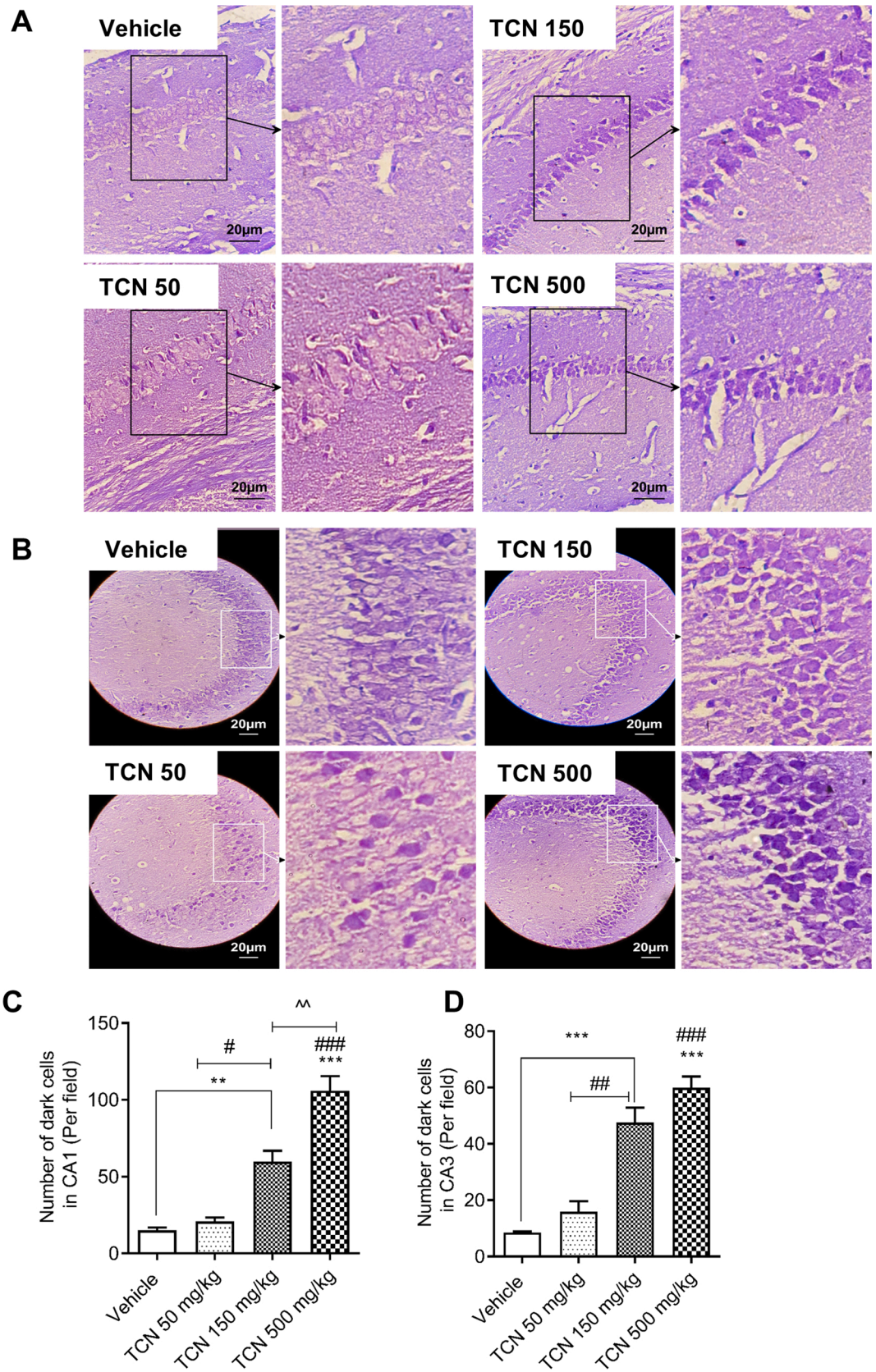

Fig. 4. Impact of TCN on number of dark neurons in CA1 and CA3 regions of hippocampus.
A–B) Representative micrographs showing Nissl staining in CA1 and CA3 regions of hippocampus. Scale bar: 20 μm.
C–D) Quantification of Nissl staining results. $^{**}P < 0.01$ and $^{***}P < 0.001$ compared to the vehicle; $^{\#}P < 0.05$, $^{\#\#}P < 0.01$, and $^{\#\#\#}P < 0.001$ compared to TCN 50 mg/kg; $^{\hat{}\hat{}}P < 0.01$ compared to TCN 150 mg/kg, n = 3.

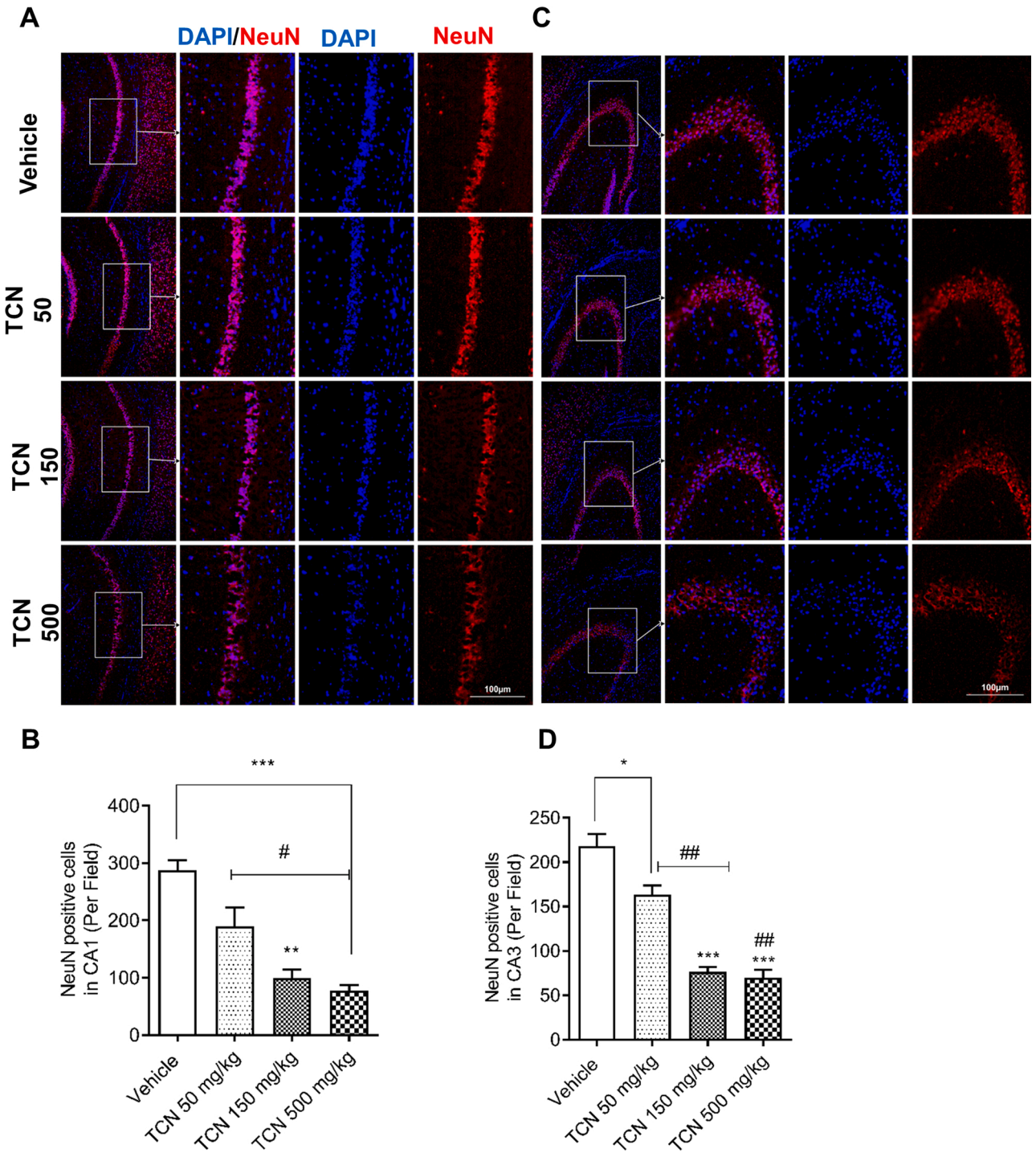

Fig. 5. Effect of TCN administration on neuronal loss in CA1 and CA3 regions of hippocampus.
A, C) Immunostaining against NeuN as neuronal marker in CA1 and CA3 regions of hippocampus. DAPI: nuclei stain, Scale bar: 100 μm.
B, D) Quantification of immunostaining results. *P < 0.05, **P < 0.01, and ***P < 0.001 compared to the vehicle; $^{\#}$P < 0.05 and $^{\#\#}$P < 0.01 compared to TCN 50 mg/kg, n = 3.

150 (P = 0.0005) and 500 mg/kg (P < 0.0001) compare with vehicle. Additionally, administration of TCN at doses of 150 and 500 mg/kg significantly exacerbated the level of astrocytes activation in CA3 region compare to dose of 50 mg/kg (P = 0.002 and P < 0.0001, respectively). A significant increase in number of GFAP positive cells was also found between TCN treated mice at doses of 150 and 500 (P = 0.008) (Fig. 7C, D).

In order to examine the impact of TCN on microglial activation, the number of Iba1 positive cells were assessed using immunostaining. Analysis of immunostaining results revealed that the number of Iba1^{+} cells significantly increased in CA1 region of TCN receiving mice at doses of 150 (P = 0.002) and 500 mg/kg (P = 0.0002) compare to vehicle group. There was also a significant increase in number of activated microglia in TCN treated mice at doses 150 (P = 0.002) and 500 mg/kg (P = 0.0002) compare to dose of 50 mg/kg (Fig. 8A, B). Furthermore, the level of microglial activation significantly exacerbated in CA3 region of TCN receiving mice at doses of 150 (P = 0.002) and 500 mg/kg (P = 0.001) compare to vehicle group. There was also a

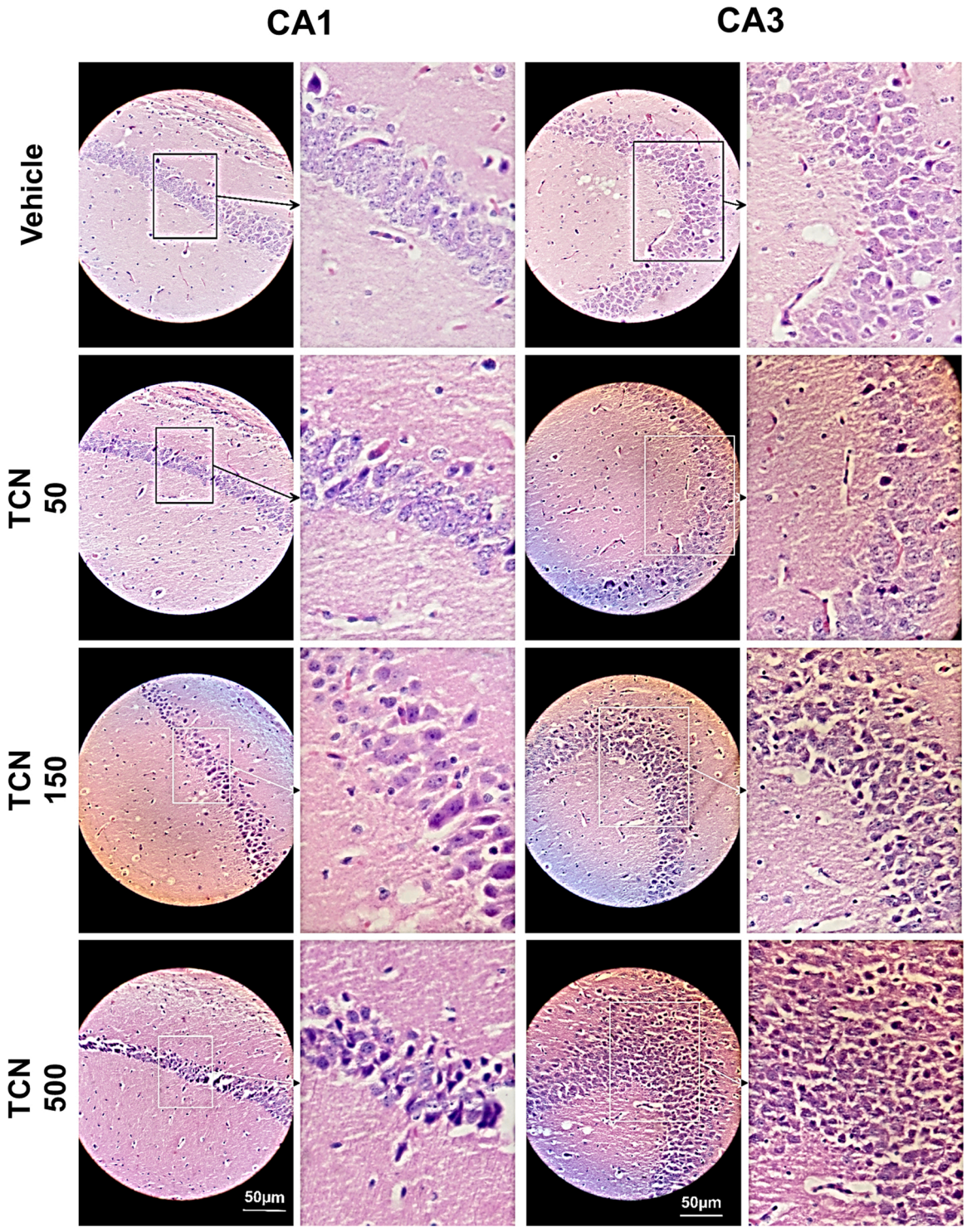

Fig. 6. Impact of TCN administration on histopathology of hippocampus.
Representative micrographs showing H&E staining in CA1 and CA3 regions of hippocampus. Scale bar: 50 μm, n = 3.

significant difference in number of Iba1 positive cells in TCN treated mice at doses 50 and 500 mg/kg (P = 0.017) (Fig. 8C, D).

4. Discussion

The neurotoxic impact of carbon nanostructures is a major obstacle in developing their biomedical applications (Hu and Gao, 2010; Teleanu et al., 2019). Gathering the previously published data, we can claim that in spite of carbon nanostructures outstanding biomedical potential, they are also potential neurotoxins (Sayapina et al., 2015, 2017; Sayapina et al., 2016; Shang et al., 2015). Utilizing a nanomaterial with desired properties and optimal biocompatibility will be the beginning of a new era in clinical applications of nanomedicine. A recently studied carbon nanomaterial, g-C3N4, has exhibited favorable properties in neuroscience along with good cellular biocompatibility *in vitro* (Chan et al., 2019; Rong et al., 2016; Zhang et al., 2013). These features prompted us to investigate its probable CNS impacts through an *in vivo* experiment (Zhang et al., 2013).

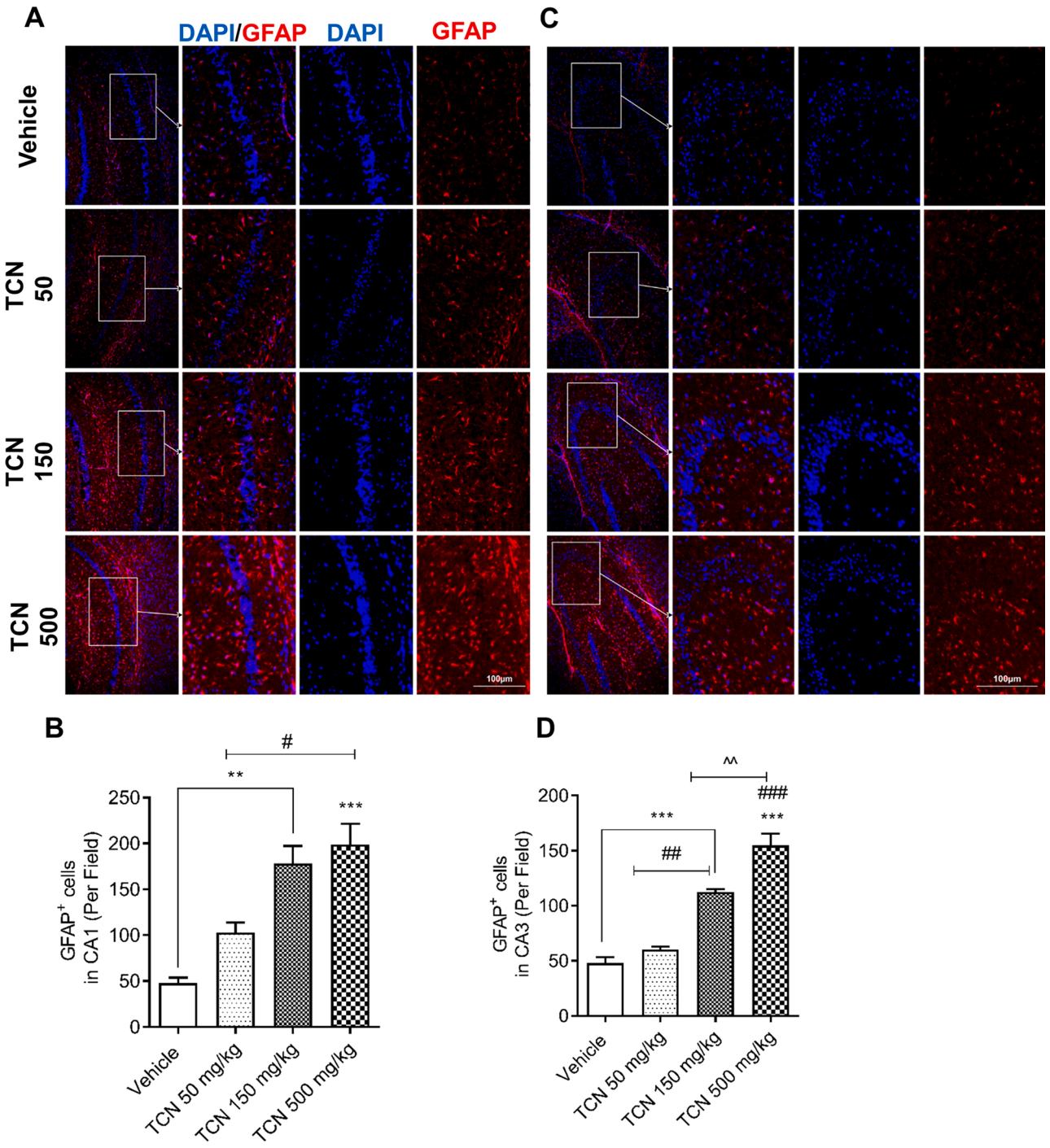

Fig. 7. Effect of TCN administration on astrocytes activation in CA1 and CA3 regions of hippocampus.
A, C) Immunostaining against GFAP as an astrocyte marker in CA1 and CA3 regions of hippocampus. DAPI: nuclei stain, Scale bar: 100 μm.
B, D) Quantification of immunostaining data. $^{**}P < 0.01$ and $^{***}P < 0.001$ compared to the vehicle; $^{\#}P < 0.05$, $^{\#\#}P < 0.01$, and $^{\#\#\#}P < 0.001$ compared to TCN 50 mg/kg, $^{\wedge\wedge}P < 0.01$ compared to TCN 150 mg/kg, n = 3.

In the present study, we were seeking TCN-induced neurobehavioral changes, its associated hippocampal neuronal damage, and possible related cellular mechanisms. We found that TCN could elicit neuronal loss and memory impairment together with increased glial activation level in a dose-dependent manner.

Based on our findings, TCN can negatively affect spatial learning and memory at the dose of 150 and 500 mg/kg. Previous studies have similarly reported cognitive deficit such as impairment in contextual fear memory following carbon nanotube stereotaxic injection to the mice, impairment in memory of zebrafish exposed to the carbon nanotube, and impairment in spatial learning and memory in mice exposed to GO in the dose-dependent manner (Da Rocha et al., 2019; Liu et al., 2014; Weber et al., 2014).

To further evaluate a part of pathophysiological events behind the observed cognitive dysfunction, we performed microscopic evaluations on hippocampal tissue. Nissl staining data demonstrated the dose-dependent toxic effect of TCN on hippocampal dark cells in CA1 and CA3 regions. The mentioned injuries were significantly observed at the dose of 150 and 500 mg/kg. Additionally, the levels of necrotic cells were increased in TCN receiving mice. In agreement with our study, a

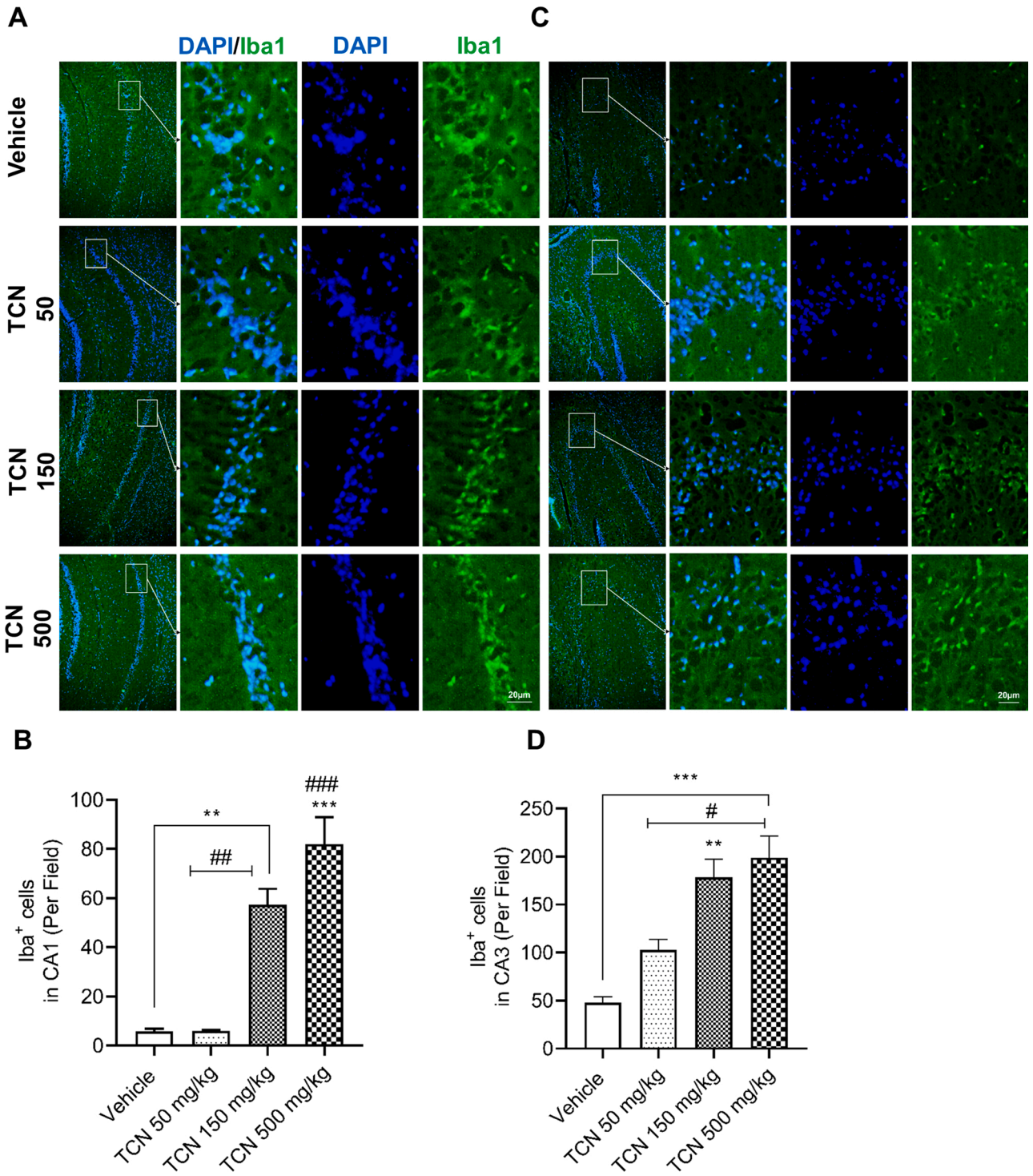

Fig. 8. Effect of TCN administration on microglial activation of hippocampus.
A, C) Immunostaining against Iba1 as a microglial marker in CA1 and CA3 regions of hippocampus. DAPI: nuclei stain, Scale bar: 20 μm.
B, D) Quantification of immunostaining data. $^{**}P < 0.01$ and $^{***}P < 0.001$ compared to the vehicle; $^{\#}P < 0.05$, $^{\#\#}P < 0.01$, and $^{\#\#\#}P < 0.001$ compared to TCN 50 mg/kg, n = 3.

study designed by Amrollahi et al. showed dose dependent necrotic changes in brain after short term intraperitoneal injection of GO (Amrollahi-Sharifabadi et al., 2018). Their injected doses were similar with our employed doses. According to their observations, histopathological changes were observed in all three GO exposed groups, prominently in 150 and 500 mg/kg GO receiving groups. Dose-dependent toxic manner was also shown following the exposure with some other carbon nanomaterials. In a study by Yang et al., they have found that carbon nanotube (CNT) could dose-dependently induce hippocampal neuronal damage, and alter the arrangement of neuronal structure in CA1 region (Liu et al., 2014).

Recent Nano toxicological approaches are widely highlighting the toxicological discipline to utilize neuroscience for investigating the cellular drug and body interaction precisely (Teleanu et al., 2019). To this aim, it is crucial to study the cellular pathway underlying the toxic behavioral and histopathological observations and consider the cellular

course of toxicity rather than several distinct mechanisms. Previous studies on the toxicity of carbon nanomaterials have clarified various cellular mechanisms related to CNS injury. There are evidence suggesting the role of mitochondrial damage, endoplasmic reticulum stress, oxidative injury, inflammation, and autophagy in carbon nanomaterial's toxicity (Amrollahi-Sharifabadi et al., 2018; Liu et al., 2014; Onoda et al., 2020; Yang et al., 2012; Yuan et al., 2019; Zhang et al., 2010, 2011). They can lead to different adverse effects like neurotransmitter changes, effects on synapses and adjacent structures (Chen et al., 2014; Da Rocha et al., 2019). Our findings show that by increasing the dose of TCN, the level of astrocyte activation dramatically increases. Activation of astrocytes and microglial cells, release of inflammatory cytokines, and granuloma formation in histopathologic evaluations are the major findings in recent studies, pointing out the role of inflammatory process in carbon nanostructures toxic impact (Amrollahi-Sharifabadi et al., 2018; Baldrighi et al., 2016; Bardi et al., 2013). We assume this correlation as a part of casualty; however, there are some issues yet to be resolved. In spite of the definite influence of inflammation on carbon nanotube and its analogous structures toxicity, there are some studies emphasizing the dual role of microglia and astrocytes in both exacerbating and mitigating the neuronal effect of carbon nanomaterials. To explain these complex data, it is necessary to note reactive astrogliosis in the neurotoxicity pathway, which is generally defined by activation of endogenous glial cells following by microglial and astrocyte activation secondary to CNS insult (Hostenbach et al., 2014). we assume that following g-C3N4 exposure to the brain, the process of glial activation embarks and induces cytokine and chemokine release, neurotransmitters, and reactive oxygen species as a consequence (Fattahi et al., 2014; Hostenbach et al., 2014). The activated astrocyte and microglia together with increased inflammatory cytokines, are supposed to protect neurons from oxidative and inflammatory insult and restrict the spread of inflammation (Costa et al., 2016; Zuidema et al., 2018). But there are some experiments showing that they can exacerbate the toxic effect of exogenous insult on neurons and increase neuronal loss, the presumed protective mechanism which turned to be an endogenous toxic process (Hostenbach et al., 2014). Some *in vitro* studies have performed and confirmed the delicate and dual role of immune cells in the toxicity pathway of carbon nanostructures. Bardi et al. showed that in mixed neuro-glial culture, CNT is predominantly internalized by glial cells (Bardi et al., 2013). In complement with their study, Belyanskaya et al. observed a dramatic increase in cytotoxicity of CNT by generating the cultures enriched in glial cells (Belyanskaya et al., 2009). There are also studies indicating that the content of a glial cells in the culture is correlated with the level of neuronal loss (Bussy et al., 2015). The preferential cytotoxicity in glial cells in comparison with neurons was also confirmed in the study by Bussy et al. (Bussy et al., 2015). On the other hand, there are some evidence showing that glial cells function and cell division can severely be affected by CNT (Villegas et al., 2014). The mentioned findings bring up two different hypotheses: 1) indirect carbon nanostructures neurotoxicity secondary to glial cells injury. 2) Neurotoxicity directly caused by toxic impact of activated microglia and astrocytes, the idea which is supported by major neuronal loss in glial rich region of the brain. Yang et al. have reported supportive evidence of the second idea in their review (Yang et al., 2020). In their study, there are some evidence regarding to the presence of two different phenotype of astrocyte with neuroprotective and neurotoxic capacity (Yang et al., 2020). Lidellow et al. named the neurotoxic astrocyte phenotype, A1 astrocyte and mentioned its major role for neurotoxic impact of immune-mediated CNS injury (Liddelow et al., 2017). They have also shown its abundance in several neurodegenerative diseases such as AD, Huntington's and Parkinson's disease (Pekny and Pekna, 2014). These findings direct us to the fact that generally expected glial cell protection capability is occur in proper microenvironment and raise the question of whether or not all the mentioned toxic events are a part of protective course preventing from inflammatory disaster. We acknowledge that our study has only clarified a part of g-C3N4 cellular effects and the detailed inflammatory events as a result of g-C3N4 can't be explained by our study design and findings. The dose-response observation and the correlated observed histopathological findings are preliminary stages of further investigations on detailed impact of g-C3N4 on inflammatory profile of the CNS in living organism. It can aid to better understanding of detailed inflammatory backbone of g-C3N4 effect on brain. Additionally, further studies with the narrower dose range are suggested to complete the toxicity profile in order to find the probable safe dose with minimal insult to preserve microenvironment fragile balance. These studies are essential for guiding the scientists to therapeutic window of this biomedical favorable carbon nanostructure.

5. Conclusion

In conclusion, the present study showed that acute administration of TCN impairs the spatial learning and memory of mice in a dose-dependent manner. Histological evaluation indicated that TCN significantly increases the levels of hippocampal neuronal loss, necrotic cells, and glial activation. Further studies are needed to examine the exact cellular and molecular mechanisms of TCN-induced neurobehavioral deficits.

Authors' contribution

Shahram Ghasemi synthetized TCN; Farangis Ramezani and Nasrin Nosratiyan collected data; Farangis Ramezani, Maryam Ghasemi-Kasman, and Farideh Feizi analyzed the results; Farangis Ramezani and Maryam Ghasemi-Kasman: Manuscript preparation; Maryam Ghasemi-Kasman designed and supervised the study.

Ethical statement

All authors have seen and approved the final version of the manuscript being submitted. They warrant that the article hasn't received prior publication and isn't under consideration for publication elsewhere. This manuscript is also in accordance with the Authorship statement of ethical standards for manuscripts submitted to Brain Research Bulletin.

Declaration of Competing Interest

The authors declare no conflict of interest related to this study.

Acknowledgments

This study was supported by a grant from the Deputy of Research and Technology (No. 724133017), Babol University of Medical Sciences, Babol, Iran and performed as a part of Medical doctor thesis.

References

Amrollahi-Sharifabadi, M., Koohi, M.K., Zayerzadeh, E., Hablolvarid, M.H., Hassan, J., Seifalian, A.M., 2018. In vivo toxicological evaluation of graphene oxide nanoplatelets for clinical application. Int. J. Nanomedicine 13, 4757–4769.

Baldrighi, M., Trusel, M., Tonini, R., Giordani, S., 2016. Carbon nanomaterials interfacing with neurons: an in vivo perspective. Front. Neurosci. 10, 250.

Bardi, G., Nunes, A., Gherardini, L., Bates, K., Al-Jamal, K.T., Gaillard, C., Prato, M., Bianco, A., Pizzorusso, T., Kostarelos, K., 2013. Functionalized carbon nanotubes in the brain: cellular internalization and neuroinflammatory responses. PLoS One 8, e80964. https://doi.org/10.1371/journal.pone.0080964.

Belyanskaya, L., Weigel, S., Hirsch, C., Tobler, U., Krug, H.F., Wick, P., 2009. Effects of carbon nanotubes on primary neurons and glial cells. Neurotoxicology 30 (4), 702–711.

Bhardwaj, V., Kaushik, A., 2017. Biomedical applications of nanotechnology and nanomaterials. Micromachines (Basel) 8, 298.

Bussy, C., Al-Jamal, K.T., Boczkowski, J., Lanone, S., Prato, M., Bianco, A., Kostarelos, K., 2015. Microglia determine brain region-specific neurotoxic responses to chemically functionalized carbon nanotubes. ACS Nano 9, 7815–7830.

Cao, L., Wang, R., Wang, D., 2015. Synthesis and characterization of sulfur self-doped g-C3N4 with efficient visible-light photocatalytic activity. Mater. Lett. 149, 50–53.

Chan, M.-H., Liu, R.-S., Hsiao, M., 2019. Graphitic carbon nitride-based nanocomposites and their biological applications: a review. Nanoscale 11 (32), 14993–15003.
Chen, T., Yang, J., Zhang, H., Ren, G., Yang, Z., Zhang, T., 2014. Multi-walled carbon nanotube inhibits CA1 glutamatergic synaptic transmission in rat's hippocampal slices. Toxicol. Lett. 229, 423–429.
Chu, X., Li, K., Guo, H., Zheng, H., Shuda, S., Wang, X., Zhang, J., Chen, W., Zhang, Y., 2017. Exploration of graphitic-C3N4 quantum dots for microwave-induced photodynamic therapy. ACS Biomater. Sci. Eng. 3, 1836–1844.
Chung, Y.J., Lee, B.I., Ko, J.W., Park, C., 2016. Photoactive g-C3N4 nanosheets for light-induced suppression of Alzheimer's β-amyloid aggregation and toxicity. Adv. Healthc. Mater. 5, 1560–1565.
Costa, P.M., Bourgognon, M., Wang, J.T., Al-Jamal, K., 2016. Functionalised carbon nanotubes: from intracellular uptake and cell-related toxicity to systemic brain delivery. J. Control. Release 241, 200–219.
Da Rocha, A., Kist, L., Almeida, E., Silva, D., Bonan, C., Altenhofen, S., Kaufmann Jr., C., Bogo, M., Barros, D., Oliveira, S., et al., 2019. Neurotoxicity in zebrafish exposed to carbon nanotubes: effects on neurotransmitters levels and antioxidant system. Comp. Biochem. Physiol. C Toxicol. Pharmacol. 218, 30–35.
Dong, Q., Mohamad Latiff, N., Mazánek, V., Rosli, N.F., Chia, H.L., Sofer, Z.k., Pumera, M., 2018. Triazine-and Heptazine-based carbon nitrides: toxicity. ACS Appl. Nano Mater. 1, 4442–4449.
Fattahi, P., Yang, G., Kim, G., Abidian, M., 2014. A review of organic and inorganic biomaterials for neural interfaces. Adv. Mater. 26, 1846–1885.
Fisher, C., E Rider, A., Jun Han, Z., Kumar, S., Levchenko, I., Ostrikov, K., 2012. Applications and nanotoxicity of carbon nanotubes and graphene in biomedicine. J. Tissue Eng. Regen. Med. 9, 1321–1338.
Gad, S.C., Cassidy, C.D., Aubert, N., Spainhour, B., Robbe, H., 2006. Nonclinical vehicle use in studies by multiple routes in multiple species. Int. J. Toxicol. 25, 499–521.
Ge, L., Han, C., Xiao, X., Guo, L., Li, Y., 2013. Enhanced visible light photocatalytic hydrogen evolution of sulfur-doped polymeric g-C3N4 photocatalysts. Mater. Res. Bull. 48, 3919–3925.
Gol, M., Ghorbanian, D., Hassanzadeh, S., Javan, M., Mirnajafi-Zadeh, J., Ghasemi-Kasman, M., 2017. Fingolimod enhances myelin repair of hippocampus in pentylenetetrazol-induced kindling model. Eur. J. Pharm. Sci. 96, 72–83.
Hashemian, M., Anissian, D., Ghasemi-Kasman, M., Akbari, A., Khalili-Fomeshi, M., Ghasemi, S., Ahmadi, F., Moghadamnia, A.A., Ebrahimpour, A., 2017.). Curcumin-loaded chitosan-alginate-STPP nanoparticles ameliorate memory deficits and reduce glial activation in pentylenetetrazol-induced kindling model of epilepsy. Prog. Neuropsychopharmacol. Biol. Psychiatry 79, 462–471.
Hashemian, M., Ghasemi-Kasman, M., Parsian, H., Sadeghi, F., 2019. Fingolimod (FTY720) improves the functional recovery and myelin preservation of the optic pathway in focal demyelination model of rat optic chiasm. Brain Res. Bull. 153, 109–121.
Hostenbach, S., Cambron, M., D'haeseleer, M., Kooijman, R., De Keyser, J., 2014. Astrocyte loss and astrogliosis in neuroinflammatory disorders. Neurosci. Lett. 565, 39–41.
Hu, Y.-L., Gao, J.-Q., 2010. Potential neurotoxicity of nanoparticles. Int. J. Pharm. 394, 115–121.
Karmakar, A., Zhang, Q., Zhang, Y., 2014. Neurotoxicity of nanoscale materials. J. Food Drug Anal. 22, 147–160.
Li, M., Guan, Y., Chen, Z., Gao, N., Ren, J., Dong, K., Qu, X., 2016. Platinum-coordinated graphitic carbon nitride nanosheet used for targeted inhibition of amyloid β-peptide aggregation. Nano Res. 9, 2411–2423.
Liddelow, S.A., Guttenplan, K.A., Clarke, L.E., Bennett, F.C., Bohlen, C.J., Schirmer, L., Bennett, M.L., Münch, A.E., Chung, W.-S., Peterson, T., 2017. Neurotoxic reactive astrocytes are induced by activated microglia. Nature 541, 481–487.
Liu, G., Niu, P., Sun, C., Smith, S.C., Chen, Z., Lu, G.Q., Cheng, H.-M., 2010. Unique electronic structure induced high photoreactivity of sulfur-doped graphitic C3N4. J. Am. Chem. Soc. 132, 11642–11648.
Liu, X., Zhang, Y., Li, J., Wang, D., Wu, Y., Li, Y., Lu, Z., Yu, S.C., Li, R., Yang, X., 2014. Cognitive deficits and decreased locomotor activity induced by single-walled carbon nanotubes and neuroprotective effects of ascorbic acid. Int. J. Nanomedicine 9, 823.
Loh, K.P., Ho, D., Chiu, G.N.C., Leong, D.T., Pastorin, G., Chow, E., 2018. Clinical applications of carbon nanomaterials in diagnostics and therapy. Adv. Mater. 30, 1802368.
Maiti, D., Tong, X., Mou, X., Yang, K., 2019. Carbon-based nanomaterials for biomedical applications: a recent study. Front. Pharmacol. 9, 1401.
Mohajeri, M., Behnam, B., Sahebkar, A., 2019. Biomedical applications of carbon nanomaterials: drug and gene delivery potentials. J. Cell. Physiol. 234, 298–319.
Naeimi, R., Safarpour, F., Hashemian, M., Tashakorian, H., Ahmadian, S.R., Ashrafpour, M., Ghasemi-Kasman, M., 2018. Curcumin-loaded nanoparticles ameliorate glial activation and improve myelin repair in lyolecithin-induced focal demyelination model of rat corpus callosum. Neurosci. Lett. 674, 1–10.
Onoda, A., Kawasaki, T., Tsukiyama, K., Takeda, K., Umezawa, M., 2020. Carbon nanoparticles induce endoplasmic reticulum stress around blood vessels with accumulation of misfolded proteins in the developing brain of offspring. Sci. Rep. 10, 1–10.
Pekny, M., Pekna, M., 2014. Astrocyte reactivity and reactive astrogliosis: costs and benefits. Physiol. Rev. 94, 1077–1098.
Rong, M., Cai, Z., Xie, L., Lin, C., Song, X., Luo, F., Wang, Y., Chen, X., 2016. Study on the ultrahigh quantum yield of fluorescent P, O-g-C3N4 nanodots and its application in cell imaging. Chemistry 22, 9387–9395.
Sayapina, N., Batalova, T., Chaika, V., Kuznetsov, V., Sergievich, A., Kolosov, V., Perel'man, Y.M., Golokhvast, K., 2015. Multi-walled carbon nanotubes increase anxiety levels in rats and reduce exploratory activity in the open field test. Dokl. Biol. Sci. 464, 223–225.
Sayapina, N.V., Sergievich, A.A., Kuznetsov, V.L., Chaika, V.V., Lisitskaya, I.G., Khoroshikh, P.P., Batalova, T.A., Tsarouhas, K., Spandidos, D., Tsatsakis, A., et al., 2016. Influence of multi-walled carbon nanotubes on the cognitive abilities of Wistar rats. Exp. Ther. Med. 12, 1311–1318.
Sayapina, N.V., Batalova, T.A., Sergievich, A.A., Shtarberg, M.A., Borodin, E.A., Khoroshikh, P.P., Chaika, V.V., Kodintsev, V.V., Vedyagin, A.A., Mishakov, I., et al., 2017. Oral application of carbon nanofibers in rats increases blood concentration of IL6 and IL10 and decreases locomotor activity. Environ. Toxicol. Pharmacol. 50, 183–191.
Shang, S., Yang, S.-Y., Liu, Z.-M., Yang, X., 2015. Oxidative damage in the kidney and brain of mice induced by different nano-materials. Front. Biol. (Beijing) 10, 91–96.
Chapter 11—The synthesis, application, and related neurotoxicity of carbon nanotubes. In: Shi, D., Mi, G., Webster, T., Jiang, X., Gao, H. (Eds.), 2017. Neurotoxicity of Nanomaterials and Nanomedicine, 1st ed, pp. 259–284.
Teleanu, D.M., Chircov, C., Grumezescu, A.M., Teleanu, R., 2019. Neurotoxicity of nanomaterials: an up-to-date overview. Nanomaterials (Basel) 9, 96.
Teradal, N.L., Jelinek, R., 2017. Carbon nanomaterials in biological studies and biomedicine. Adv. Healthc. Mater. 6, 1700574.
Tian, J., Liu, Q., Ge, C., Xing, Z., Asiri, A.M., Al-Youbi, A.O., Sun, X., 2013. Ultrathin graphitic carbon nitride nanosheets: a low-cost, green, and highly efficient electrocatalyst toward the reduction of hydrogen peroxide and its glucose biosensing application. Nanoscale 5 (19), 8921–8924.
Tian, N., Huang, H., Guo, Y., He, Y., Zhang, Y., 2014. A g-C3N4/Bi2O2CO3 composite with high visible-light-driven photocatalytic activity for rhodamine B degradation. Appl. Surf. Sci. 322, 249–254.
Villegas, J.C., Álvarez-Montes, L., Rodríguez-Fernández, L., González, J., Valiente, R., Fanarraga, M., 2014. Multiwalled carbon nanotubes hinder microglia function interfering with cell migration and phagocytosis. Adv. Healthc. Mater. 3, 424–432.
Vinoth, S., Rajaitha, P.M., Venkadesh, A., Devi, K.S., Radhakrishnan, S., Pandikumar, A., 2020. Nickel sulfide-incorporated sulfur-doped graphitic carbon nitride nanohybrid interface for non-enzymatic electrochemical sensing of glucose. Nanoscale Adv. 2 (9), 4242–4250.
Wang, J., Yang, M., 2019. Two-dimensional nanomaterials in cancer theranostics. Theranostic Bionanomaterials, pp. 263–288.
Wang, A.-J., Li, H., Huang, H., Qian, Z.-S., Feng, J.-J., 2016. Fluorescent graphene-like carbon nitrides: synthesis, properties and applications. J. Mater. Chem. C Mater. Opt. Electron. Devices 4, 8146–8160.
Wang, Y., Tian, Y., Yan, L., Su, Z., 2018. DFT study on sulfur-doped g-C3N4 nanosheets as a photocatalyst for CO2 reduction reaction. J. Phys. Chem. C. 122, 7712–7719.
Weber, G.E., Dal Bosco, L., Gonçalves, C.O., Santos, A.P., Fantini, C., Furtado, C.A., Parfitt, G.M., Peixoto, C., Romano, L.A., Vaz, B., et al., 2014. Biodistribution and toxicological study of PEGylated single-wall carbon nanotubes in the zebrafish (Danio rerio) nervous system. Toxicol. Appl. Pharmacol. 280, 484–492.
Xiong, M., Rong, Q., Meng, H.-m., Zhang, X., 2017. Two-dimensional graphitic carbon nitride nanosheets for biosensing applications. Biosens. Bioelectron. 89, 212–223.
Yang, S.-T., Luo, J., Zhou, Q., Wang, H.J.T., 2012. Pharmacokinetics, metabolism and toxicity of carbon nanotubes for biomedical purposes. Theranostics 2 (3), 271.
Yang, T., Dai, Y., Chen, G., Cui, S., 2020. Dissecting the dual role of the glial scar and scar-forming astrocytes in spinal cord injury. Front. Cell. Neurosci. 14, 78.
Yuan, X., Zhang, X., Sun, L., Wei, Y., Wei, X., 2019. Cellular toxicity and immunological effects of carbon-based nanomaterials. Part. Fibre Toxicol. 16, 18.
Zhang, Y., Ali, S.F., Dervishi, E., Xu, Y., Li, Z., Casciano, D., Biris, A., 2010. Cytotoxicity effects of graphene and single-wall carbon nanotubes in neural phaeochromocytoma-derived PC12 cells. ACS Nano 4, 3181–3186.
Zhang, Y., Xu, Y., Li, Z., Chen, T., Lantz, S.M., Howard, P.C., Paule, M.G., Slikker Jr., W., Watanabe, F., Mustafa, T., 2011. Mechanistic toxicity evaluation of uncoated and PEGylated single-walled carbon nanotubes in neuronal PC12 cells. ACS Nano 5, 7020–7033.
Zhang, G., Zhang, J., Zhang, M., Wang, X., 2012. Polycondensation of thiourea into carbon nitride semiconductors as visible light photocatalysts. J. Mater. Chem. 22, 8083–8091.
Zhang, X., Xie, X., Wang, H., Zhang, J., Pan, B., Xie, Y., 2013. Enhanced photoresponsive ultrathin graphitic-phase C3N4 nanosheets for bioimaging. J. Am. Chem. Soc. 135, 18–21.
Zhang, L., Liu, C., Wang, Q., Wang, X., Wang, S., 2020. Electrochemical sensor based on an electrode modified with porous graphitic carbon nitride nanosheets (C 3 N 4) embedded in graphene oxide for simultaneous determination of ascorbic acid, dopamine and uric acid. Mikrochim. Acta 187 (2), 149.
Zuidema, J.M., Gilbert, R.J., Gottipati, M., 2018. Biomaterial approaches to modulate reactive astroglial response. Cells Tissues Organs 205 (5-6), 372–395.